Motion-Estimation-Based Visual Servoing of Nonholonomic Mobile Robots

Xuebo Zhang, Yongchun Fang, and Xi Liu

***Abstract*—A 2-1/2-D visual servoing strategy, which is based on a novel motion-estimation technique, is presented for the stabilization of a nonholonomic mobile robot (which is also called the "parking problem"). By taking into account the planar motion constraint of mobile robots, the proposed motion-estimation technique can be applied in both planar and nonplanar scenes. In addition, this approach requires no matrix estimation or decomposition, and it avoids ambiguity and degeneracy problems for the homography or fundamental matrix-based algorithms. Moreover, the field-of-view (FOV) constraint of the onboard camera is largely alleviated because the presented algorithm works well with few feature points. In order to incorporate the advantages of position-based visual servoing and image-based visual servoing, a composite error vector is defined that includes both image signals and the estimated rotational angle. Subsequently, a smooth time-varying feedback controller is adopted to cope with the nonholonomic constraints, which yields global exponential convergent rate for the closed-loop system. On the basis of the perturbed linear system theory, we show that practical exponential stability can be achieved, despite the lack of depth information, which is inherent for monocular camera systems. Both simulation and experiment results are collected to investigate the feasibility of the proposed approach.**

***Index Terms*—Field of view (FOV), motion control, planar motion estimation, visual servoing, wheeled robots.**

I. Introduction

Visual servoing takes account of using visual feedback to drive a robot from an initial configuration to the desired one, which is defined by a previously acquired image with a pinhole camera. Traditionally, research on visual servoing has focused on six-degree-of-freedom robot manipulators [1]–[3], wherein motion constraints are generally not considered. However, mobile robots are usually subject to nonholonomic constraints, which brings even more challenges for the visual servoing tasks because nonholonomic systems cannot be asymptotically stabilized by any time-invariant continuous state feedback control law, as clearly demonstrated by the well-known Brockett necessary condition [4]. Besides, the lack of depth information has been an inherent problem for monocular camera-based vision systems, for which the robot state cannot be exactly/completely reconstructed with unknown 3-D model of the target. Consequently, visual servoing of nonholonomic mobile robots is even more difficult because of motion constraints and unknown depth information. During the past decades, various control design strategies, such as discontinuous approaches [5], [6], smooth time-varying control laws [7]–[10], or a combination of them [11], [12], have been developed, respectively, to obtain satisfactory control performance for nonholonomic systems. However, these techniques cannot take the vision system into the feedback loop, and it is assumed that full state feedback is available, which is clearly not true for visual servoing systems because of unknown depth information.

Position-based visual servoing (PBVS) of mobile robots has been investigated in the literature to reduce the visual servoing task to a control problem in the Cartesian space [13]–[16]. In [16], Murrieri *et al*. propose a hybrid control approach that is based on polar coordinates [17] and Lyapunov theory to address the parking problem of a nonholonomic mobile robot, which can successfully keep the features in the camera field of view (FOV) during the visual servoing process. However, these approaches require some 3-D metric information of the features known as *a priori*, which is further used to reconstruct full-system state for feedback control.

Recently, an image-based visual servoing (IBVS) strategy is proposed in [18] by computation of the epipolar geometry, based on which a two-step control scheme is designed to drive the mobile robot to the desired configuration. Unfortunately, short baseline degeneracies occasionally happen during the visual servoing process since there is no direct control on the distance between the current and desired positions, especially when the initial configuration is close to the desired one. In order to cope with this problem, López-Nicolás *et al*. [19] introduce an auxiliary fundamental matrix by use of another image at the last stage of motion to avoid the degeneracies in the epipole-based control. Most recently, they have proposed a novel direct visual servoing approach that is based on the use of the essential matrix, which can cope with the short baseline degeneracy by the introduction of a virtual target [20] and the use of the input–output linearization of the system. Nevertheless, to compute the epipolar geometry, many feature points (generally, eight or more) are usually required for general fundamental matrix-estimation techniques, such as the well-known eight-point algorithm [21]. Moreover, the epipolar geometry becomes ill conditioned if all the points lie on the same planar scene, which is quite usual in human environments.

A feasible way to overcome problems of the epipolar geometry is to use the planar homography such as given in [22] and [23]. In [22], Fang *et al*. exploit the homography decomposition technique to obtain the relative orientation and the scaled Euclidean position, based on which a periodic time-varying adaptive control law is proposed to asymptotically regulate the mobile robot to its desired pose. However, the homography estimation requires that all the features are coplanar, and the decomposition process is not a trivial issue [24], in which singular value decomposition (SVD) is required, and two possible solutions are obtained in general case. In order to simplify this pose-estimation strategy, an analytical method is proposed to decompose the Euclidean homography in the previous work [25]. This approach does not require SVD, and it meets no ambiguity problem in general case. In [26], to avoid the issue of homography decomposition, elements of the estimated homography are formulated as the output of the system, based on which a control law is designed by the input–output linearization technique (a similar technique for essential matrix-based visual servoing can be found in [20]). Although these techniques simplify or avoid the homography decomposition, they still need to carry out the homography estimation as the first procedure. In addition, when the features are not coplanar, the homography-based approach cannot be applied. Thus, it is still an open problem to compute the relative pose directly from feature correspondences without matrix estimation in both planar or nonplanar scenes.

To directly compute the relative pose from images, a novel motion-estimation methodology is first proposed in our preliminary study [27] by using correspondences of three unknown feature points in two images. This technique does not require homography/fundamental matrix

Manuscript received December 28, 2010; revised April 20, 2011; accepted July 13, 2011. Date of publication August 18, 2011; date of current version December 8, 2011. This paper was recommended for publication by the Associate Editor K. Kyriakopoulos and Editor G. Oriolo upon evaluation of the reviewers' comments. This work was supported in part by the Chinese Research Fund for the Doctoral Program of Higher Education under Grant 20090031110035 and in part by the National Natural Science Foundation of China under Grant 60875055.

The authors are with are with the Institute of Robotics and Automatic Information Systems, Nankai University, Tianjin 300071, China (e-mail: zhangxb@robot.nankai.edu.cn; yfang@robot.nankai.edu.cn; liux@robot.nankai.edu.cn).

Color versions of one or more of the figures in this paper are available online at http://ieeexplore.ieee.org.

Digital Object Identifier 10.1109/TRO.2011.2162765

estimation or decomposition, and it causes no ambiguity problem. Furthermore, it is shown that even only two feature points remain in the camera FOV during the visual servoing process, the relative pose can still be correctly extracted based on the continuity property of the robot motion. Based on this motion-estimation method, a 2-1/2-D visual servoing strategy is proposed to regulate a nonholonomic mobile robot with an onboard camera to its target pose, which is specified through a desired image. To incorporate the advantages of IBVS and PBVS, the system error vector is defined as a combination of both image signals and the estimated rotational angle. Inspired by the work for the stabilization of chained systems that appeared in [9], a time-varying smooth state feedback controller is constructed to stabilize the nonholonimic mobile robot to its desired pose exponentially fast, despite the nonholonomic constraint and unknown depth information. The theory from perturbed linear systems is adopted to show the practical exponential stability of the closed-loop system. Finally, both simulation and experimental results are provided to validate the motion-estimation-based visual servoing approach. The main contribution of this paper includes the following: 1) The proposed motion-estimation technique can be applied in both planar and nonplanar scenes, and it only needs three features to obtain a unique solution; 2) even in the presence of only two visible feature points, the right solution can be obtained by using the continuity of motion to eliminate the ambiguity problem, and hence, a byproduct is that the FOV constraint of the visual camera is partially alleviated; and 3) a novel composite error system is developed, based on which a 2-1/2-D time-varying control design methodology can be adopted to cope with the nonholonomic constraints, despite the lack of depth information.

The rest of this paper is organized as follows. Section II formulates the visual servoing problem that is considered in this paper. Section III introduces a new motion-estimation strategy from two images. The system model and controller design are developed in Sections IV and V, respectively. Simulation and experimental results are provided in Section VI. This paper is concluded in Section VII.

II. Problem Statement

A. Problem Formulation

In this paper, we consider a differential drive mobile robot that is equipped with an onboard camera. As shown in Fig. 1, let $\mathcal{F}$ denote the orthogonal coordinate system that is attached to the camera, with its origin O being located at the camera center. The z-axis passes through the midpoint of the wheels axis that is orthogonal to the motion plane of the mobile robot, and the x-axis of $\mathcal{F}$ is along the optical axis that is supposed to be aligned with the front of the mobile robot. In addition, we define another orthogonal coordinate system $\mathcal{F}^*$ to represent the desired/target pose of the camera. Furthermore, it is assumed that three feature points in the scene can be extracted from the images for the visual servoing task. Hence, the objective is to regulate the nonholonomic mobile robot to its desired pose by image feedback such that $\mathcal{F}$ and $\mathcal{F}^*$ are coincident with each other.

B. Basic Notation

Consider N static feature points $\mathcal{P}_i (i = 1, 2, 3, \ldots, N)$ in the scene, with $\boldsymbol{P}_i$, $\boldsymbol{P}_i^* \in \mathbb{R}^3$ being the 3-D Euclidean coordinates that are described in the frames $\mathcal{F}$ and $\mathcal{F}^*$, respectively, as follows:

$$\boldsymbol{P}_i = [X_i,\, Y_i,\, Z_i]^T, \quad \boldsymbol{P}_i^* = [X_i^*,\, Y_i^*,\, Z_i^*]^T. \tag{1}$$

The corresponding homogeneous image pixel coordinates $\boldsymbol{p}_i, \boldsymbol{p}_i^* \in \mathbb{R}^3$ are expressed as

$$\boldsymbol{p}_i = [1,\, u_i,\, v_i]^T, \quad \boldsymbol{p}_i^* = [1,\, u_i^*,\, v_i^*]^T. \tag{2}$$

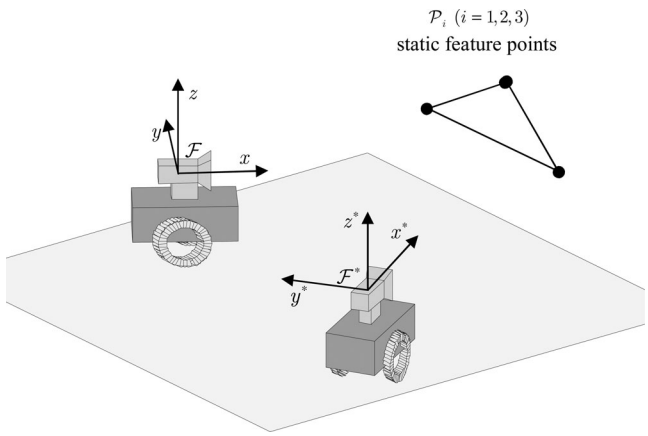

Fig. 1. Coordinate systems relationship.

It is clear that the image pixel coordinates are related to the Euclidean position of the point $\mathcal{P}_i$ through a pinhole camera model as follows:

$$\boldsymbol{p}_i = \frac{1}{X_i} A \boldsymbol{P}_i, \quad \boldsymbol{p}_i^* = \frac{1}{X_i^*} A \boldsymbol{P}_i^* \tag{3}$$

where $A \in \mathbb{R}^{3\times 3}$ denotes the intrinsic camera matrix that can be determined by camera calibration techniques [28].

To facilitate subsequent analysis, we define the following normalized image coordinates $\boldsymbol{m}_i, \boldsymbol{m}_i^* \in \mathbb{R}^3$:

$$\boldsymbol{m}_i = [1, y_i, z_i]^T = \frac{1}{X_i} \boldsymbol{P}_i$$
$$\boldsymbol{m}_i^* = [1, y_i^*, z_i^*]^T = \frac{1}{X_i^*} \boldsymbol{P}_i^*. \tag{4}$$

Based on (3) and (4), it is easy to obtain

$$\boldsymbol{m}_i = A^{-1} \boldsymbol{p}_i, \quad \boldsymbol{m}_i^* = A^{-1} \boldsymbol{p}_i^*. \tag{5}$$

That is, from the image pixel coordinates, we can calculate the normalized image coordinates $\boldsymbol{m}_i$ and $\boldsymbol{m}_i^*$, which will be further used by the motion-estimation algorithm that is described in Section III.

III. Motion Estimation From Two Images

Vision-based motion estimation from two views has been investigated widely in the computer vision community, where the problem is also termed as "structure from motion" or "relative pose problem" in the literature [24], [29]. The homography matrix algorithm and the essential matrix algorithm are mostly utilized in the visual servoing framework [30]. All aforementioned works focus on 3-D unconstrained motion estimation. In this paper, the planar motion constraint of the mobile robot is taken into account, and hence, a novel 2-D motion-estimation technique is developed to extract the relative pose, which can be directly computed from correspondences of feature points from two views and then utilized to facilitate the subsequent design of a 2-1/2-D visual servoing strategy.

From pixel coordinates, it is shown in Section II-B that the camera model is used to compute normalized image coordinates, based on which the motion-estimation algorithm is described in detail in Section III-A to extract the relative pose for the feedback control.

A. Motion-Estimation Algorithm

A motion-estimation algorithm is proposed by considering the planar motion constraint of the mobile robot. A criterion is provided to judge

if a unique solution can be computed, while degeneracy cases of the proposed algorithm are discussed in the end of this section.

The planar motion of a mobile robot is described in terms of a rotation matrix $R \in \mathbb{R}^{3\times3}$ and a translation vector $\boldsymbol{T} \in \mathbb{R}^3$ as follows:

$$R = \begin{bmatrix} \cos(\theta) & -\sin(\theta) & 0 \\ \sin(\theta) & \cos(\theta) & 0 \\ 0 & 0 & 1 \end{bmatrix}, \quad \boldsymbol{T} = \begin{bmatrix} t_x \\ t_y \\ 0 \end{bmatrix} \tag{6}$$

where $\theta \in \mathbb{R}$ is referred to as the rotation angle around the z-axis.

Therefore, the motion-estimation problem can be defined as follows: The inputs of the algorithm are the normalized image coordinates $\boldsymbol{m}_i$ and $\boldsymbol{m}_i^*$, which can be directly computed from pixel coordinates by using (5) in spite of unknown depth information X_i, X_i^*, while the outputs of the algorithm are the scaled relative motion between the current and the desired pose, that is, the rotation R and the scale translation $\boldsymbol{T}/X_i^*$.

From simple geometric analysis, it is clear that

$$\boldsymbol{P}_i = R\boldsymbol{P}_i^* + \boldsymbol{T}. \tag{7}$$

After substituting (1) into (7), the following relationship can be derived:

$$\begin{bmatrix} X_i \\ Y_i \\ Z_i \end{bmatrix} = \begin{bmatrix} X_i^*\cos(\theta) - Y_i^*\sin(\theta) + t_x \\ X_i^*\sin(\theta) + Y_i^*\cos(\theta) + t_y \\ Z_i^* \end{bmatrix}. \tag{8}$$

Hence, it is easy to obtain

$$\frac{Y_i}{X_i} = \frac{X_i^*\sin(\theta) + Y_i^*\cos(\theta) + t_y}{X_i^*\cos(\theta) - Y_i^*\sin(\theta) + t_x} \tag{9}$$

$$\frac{Z_i}{X_i} = \frac{Z_i^*}{X_i^*\cos(\theta) - Y_i^*\sin(\theta) + t_x}. \tag{10}$$

Using (4), we can rewrite (9) and (10) as follows:

$$y_i = \frac{\sin(\theta) + y_i^*\cos(\theta) + (t_y/X_i^*)}{\cos(\theta) - y_i^*\sin(\theta) + (t_x/X_i^*)} \tag{11}$$

$$z_i = \frac{z_i^*}{\cos(\theta) - y_i^*\sin(\theta) + (t_x/X_i^*)}. \tag{12}$$

Suppose $z_i \neq 0$ in the analysis (the situation of $z_i = 0$ will be discussed as degeneracy cases at the end of this section), we have

$$y_i \cdot \frac{z_i^*}{z_i} = \sin(\theta) + y_i^*\cos(\theta) + \frac{t_y}{X_i^*} \tag{13}$$

$$\frac{z_i^*}{z_i} = \cos(\theta) - y_i^*\sin(\theta) + \frac{t_x}{X_i^*}. \tag{14}$$

Therefore, the following two constraints can be obtained:

$$\frac{t_y}{X_i^*} = y_i \cdot \frac{z_i^*}{z_i} - \sin(\theta) - y_i^*\cos(\theta) \tag{15}$$

$$\frac{t_x}{X_i^*} = \frac{z_i^*}{z_i} - \cos(\theta) + y_i^*\sin(\theta). \tag{16}$$

In a similar way, corresponding constraints for the point $\mathcal{P}_j$ can be implied:

$$\frac{t_y}{X_j^*} = y_j \cdot \frac{z_j^*}{z_j} - \sin(\theta) - y_j^*\cos(\theta) \tag{17}$$

$$\frac{t_x}{X_j^*} = \frac{z_j^*}{z_j} - \cos(\theta) + y_j^*\sin(\theta). \tag{18}$$

From (15) and (18), it is easy to show that

$$\frac{t_x t_y}{X_i^* X_j^*} = \left[y_i \frac{z_i^*}{z_i} - \sin(\theta) - y_i^*\cos(\theta) \right] \cdot \left[\frac{z_j^*}{z_j} - \cos(\theta) + y_j^*\sin(\theta) \right]. \tag{19}$$

From (16) and (17), we can obtain

$$\frac{t_x t_y}{X_i^* X_j^*} = \left[\frac{z_i^*}{z_i} - \cos(\theta) + y_i^*\sin(\theta) \right] \cdot \left[y_j \cdot \frac{z_j^*}{z_j} - \sin(\theta) - y_j^*\cos(\theta) \right]. \tag{20}$$

Utilizing (19) and (20), and after some calculation, the following relationship can be derived:

$$a_{ij}\sin(\theta) + b_{ij}\cos(\theta) + c_{ij} = 0 \tag{21}$$

where $a_{ij}, b_{ij}, c_{ij} \in \mathbb{R}$ are defined as

$$a_{ij} = \frac{z_i^*}{z_i}(y_i y_j^* + 1) - \frac{z_j^*}{z_j}(y_i^* y_j + 1) \tag{22}$$

$$b_{ij} = \frac{z_j^*}{z_j}(y_j - y_i^*) - \frac{z_i^*}{z_i}(y_i - y_j^*) \tag{23}$$

$$c_{ij} = (y_i - y_j)\frac{z_i^* z_j^*}{z_i z_j} + (y_i^* - y_j^*). \tag{24}$$

Given that only two features $\mathcal{P}_1$ and $\mathcal{P}_2$ are available such that $z_i \neq 0 (i = 1, 2)$ and not all of the three coefficients a_{12}, b_{12}, and c_{12} are zero, then it follows from (21) that

$$a_{12}\sin(\theta) + b_{12}\cos(\theta) + c_{12} = 0. \tag{25}$$

By further employment of the fact that

$$\sin^2(\theta) + \cos^2(\theta) = 1 \tag{26}$$

we obtain two groups of solutions for $\sin(\theta)$ or $\cos(\theta)$ by substituting (25) into (26) and then solving a quadratic equation. Unfortunately, there is no effective way to discriminate the right solution from the wrong one, because of the lack of knowledge about the depth X_i and X_i^*. However, during the visual servoing process, the correct solution can be obtained by use of the continuity property of the robot motion, even in the case that only two feature points are available (for instance, the third point escapes from the camera FOV). In this regard, the presented algorithm gains some robustness with respect to the FOV constraint.

Given $N \geq 3$ feature points $\mathcal{P}_i (i = 1, 2, \ldots, N)$, (21) can be rewritten as

$$\begin{bmatrix} a_{ij} & b_{ij} \end{bmatrix} \begin{bmatrix} \xi_1 \\ \xi_2 \end{bmatrix} = -c_{ij} \tag{27}$$

with $\xi_1 = \sin(\theta)$, and $\xi_2 = \cos(\theta)$. If the following rank condition holds:

$$\text{Rank} \begin{bmatrix} a_{12} & b_{12} \\ a_{13} & b_{13} \\ \cdots & \cdots \\ a_{1N} & b_{1N} \end{bmatrix} = 2 \tag{28}$$

then by stacking together (27) for all feature points, the standard linear least-squares method can be adopted to obtain a unique solution. Thus, an initial estimate of θ can be computed as $\hat{\theta} = \text{atan2}(\xi_1, \xi_2)$, based on which an initial estimate of the translation vector $\boldsymbol{T}/X_i^*$

is obtained by using (15) and (16). Let $t_{\rm dsi} = \|\boldsymbol{T}/X_i^*\|$ and $\theta_t = \mathrm{atan2}(t_y/X_i^*, t_x/X_i^*)$ denote the magnitude and the orientation of $\boldsymbol{T}/X_i^*$, respectively; hence, the initial estimates of $t_{\rm dsi}$ and θ_t are calculated as $\hat{t}_{\rm dsi}$ and $\hat{\theta}_t$. The parameters $\hat{\theta}, \hat{t}_{\rm dsi}$, and $\hat{\theta}_t$ will be utilized as the initial guess for the subsequent nonlinear optimization process by minimizing the projection error $\boldsymbol{J}(\hat{\theta}, \hat{\theta}_t, \hat{t}_{\rm dsi})$ in image space

$$\boldsymbol{J}(\hat{\theta}, \hat{\theta}_t, \hat{t}_{\rm dsi}) = \sum_{i=1}^{N} \Big\{ \big(y_i - \hat{y}_i(\hat{\theta}, y_i^*, z_i^*, \hat{\theta}_t, \hat{t}_{\rm dsi})\big)^2 + \big(z_i - \hat{z}_i(\hat{\theta}, y_i^*, z_i^*, \hat{\theta}_t, \hat{t}_{\rm dsi})\big)^2 \Big\} \tag{29}$$

where $\hat{y}_i$ and $\hat{z}_i$ are computed by the substitution of $\theta = \hat{\theta}, t_y/X_i^* = \hat{t}_{\rm dsi}\sin\theta_t, t_x/X_i^* = \hat{t}_{\rm dsi}\cos\theta_t$ into (11) and (12). Subsequently, the Levenberg–Marquart algorithm [28] is further adopted to yield the final optimized estimation for $\theta, t_x/X_i^*$, and t_y/X_i^*.

Remark 1: Degeneracy cases exist for most of the estimation algorithms [21] in the field of computer vision, for which some mathematical criteria, such as (28), are used other than a condition on physical location of the 3-D features. To describe the algorithm more clearly, some necessary physical requirements for feature location are stated (note that these requirements for the proposed method are only part of the requirements for the homography- or the epipolar geometry-based method, which can be shown through some mathematical analysis.). To ensure the existence of the solution, at least two feature points with nonzero z_i coordinates are required, and these two features are not lying on the same perpendicular line with respect to the motion plane of the mobile robot (see Property 1 in the Appendix). To obtain a unique solution, it is generally required that there exist three feature points that do not lie in the same perpendicular plane with respect to the motion plane of the mobile robot (refer to Property 2 in the Appendix).

IV. Open-Loop Syatem Development

Because of the planar motion of the mobile robot, the following relationship holds for any feature point $\mathcal{P}_i$:

$$Z_i = Z_i^*. \tag{30}$$

That is, the height information Z_i remains constant during the visual servoing process.

For convenience, we define an auxiliary signal $\boldsymbol{s} \in \mathbb{R}^2$ as follows:

$$\boldsymbol{s} = [y_i, z_i]^{\rm T} = \left[\frac{Y_i}{X_i}, \frac{Z_i}{X_i}\right]^{\rm T} \tag{31}$$

where y_i and z_i are entries of the normalized image coordinates $\boldsymbol{m}_i$ that are defined in (4). It is known that the velocity of the feature point in the image space is related to the camera spatial velocity as follows:

$$\dot{\boldsymbol{s}} = L\boldsymbol{v}_c \tag{32}$$

where $\boldsymbol{v}_c = [v, w]^{\rm T} \in \mathbb{R}^2$, with v and w denoting the linear and angular velocities of the onboard camera, respectively, and where $L \in \mathbb{R}^{2\times 2}$ is the image Jacobian matrix, which is defined as

$$L = \begin{bmatrix} \dfrac{y_i}{X_i} & -(1+y_i^2) \\ \dfrac{z_i}{X_i} & -y_i z_i \end{bmatrix} \tag{33}$$

where $X_i \in \mathbb{R}$ is referred to as the depth information.

Motivated by the specific form of (13) and (14) in the motion-estimation process, we introduce the following two state variables as

$$\rho_1 = \frac{y_i}{z_i}, \quad \rho_2 = \frac{1}{z_i}. \tag{34}$$

By utilizing (32), (33), and (34), the kinematics model is obtained as

$$\dot{\rho}_1 = -\rho_2 w \tag{35}$$

$$\dot{\rho}_2 = -\frac{1}{X_i(t)}\rho_2 v + \rho_1 w. \tag{36}$$

Using (31) and (34), it is clear that

$$\frac{1}{X_i(t)}\rho_2 = \frac{1}{X_i(t)} \cdot \frac{X_i(t)}{Z_i} = \frac{1}{Z_i}. \tag{37}$$

Consequently, the time-varying unknown depth information $X_i(t)$ is related to an unknown constant Z_i in (30), which brings much convenience for subsequent controller design as shown in Section V. Thus, (35) and (36) can be rewritten as

$$\dot{\rho}_1 = -\rho_2 w \tag{38}$$

$$\dot{\rho}_2 = -\frac{1}{Z_i} v + \rho_1 w. \tag{39}$$

It can be shown from (13) and (14) that when the system state $\rho_1(t) \to \rho_1^*, \rho_2(t) \to \rho_2^*, \theta(t) \to 0$, $\mathcal{F}$ and $\mathcal{F}^*$ will be coincident with each other, wherein ρ_1^* and $\rho_2^* \in \mathbb{R}$ are defined as follows:

$$\rho_1^* = \frac{y_i^*}{z_i^*}, \quad \rho_2^* = \frac{1}{z_i^*} \tag{40}$$

which can be directly computed through the camera model from the desired image by using (5). Therefore, the objective of the visual servoing task becomes construction of suitable velocities v and w to ensure that

$$\rho_1(t) \to \rho_1^*, \rho_2(t) \to \rho_2^*, \theta(t) \to 0. \tag{41}$$

To facilitate the subsequent controller design, the error signals are defined as follows:

$$\begin{bmatrix} e_1 \\ e_2 \end{bmatrix} = \begin{bmatrix} \rho_1 \\ \rho_2 \end{bmatrix} - \begin{bmatrix} \cos(\theta) & -\sin(\theta) \\ \sin(\theta) & \cos(\theta) \end{bmatrix} \begin{bmatrix} \rho_1^* \\ \rho_2^* \end{bmatrix} \tag{42}$$

and

$$e_0 = \theta. \tag{43}$$

After taking the time derivative of the error signals and substituting (38) and (39) into them, the open-loop error system is obtained

$$\dot{e}_0 = w \tag{44}$$

$$\dot{e}_1 = -e_2 w \tag{45}$$

$$\dot{e}_2 = -\frac{1}{Z_i} v + e_1 w. \tag{46}$$

V. Control Development

Inspired by the control design methods for chained nonholonomic systems [9], [10], a smooth time-varying pure feedback controller is proposed to regulate the mobile robot to its desired pose exponentially fast, and it is further shown that the controller design is independent of the unknown height Z_i that is related to the time-varying unknown depth information as shown in (37).

The basic idea of this design methodology is to partition the whole system of (44)–(46) into the following two subsystems Σ_1 and Σ_2:

$$\Sigma_1 : \dot{e}_0 = w \tag{47}$$

$$\Sigma_2 : \begin{cases} \dot{e}_1 = -e_2 w \\ \dot{e}_2 = -\dfrac{1}{Z_i} v + e_1 w \end{cases} \tag{48}$$

and then, a proper control law for each subsystem is designed that finally stabilizes the overall closed-loop system.

From linear system control theory, it is clear that a simple proportional state feedback controller of $w = -k_0 e_0(t)$ ($k_0 \in \mathbb{R}$ is a positive control gain) can be easily constructed to guarantee the stability of the state $e_0(t)$. However, if the initial state of the system is on the singular manifold, namely $e_0(0) = 0$, then the corresponding control input $w = 0$ will make the second system Σ_2 uncontrollable. Hence, an explicit exponential decaying term is combined to drive the system state away from the singular manifold. Based on the previous analysis, the control input w is designed as

$$w = -k_0 e_0 + \lambda e^{-\alpha t} \tag{49}$$

where $k_0, \alpha \in \mathbb{R}$ are positive constants, and $\lambda \in \mathbb{R}$ is a nonzero constant that represents the weight of the disturbance term. After the substitution of (49) into (47), the trajectory of $e_0(t)$ can be easily obtained by solving a first-order differential equation

$$e_0(t) = \frac{\lambda}{k_0 - \alpha} e^{-\alpha t} + \left(e_0(0) - \frac{\lambda}{k_0 - \alpha} \right) e^{-k_0 t}. \tag{50}$$

From (49) and (50), it is easy to show that

$$e_0(t), w(t) \longrightarrow 0 \text{ exponentially fast.} \tag{51}$$

To facilitate the subsequent controller design, a state transformation is introduced as follows:

$$\begin{cases} r_1 = e_2 \\ r_2 = e_1 e^{\alpha t}. \end{cases} \tag{52}$$

Hence, the system model with new state $\boldsymbol{r} = [r_1(t), r_2(t)]^T$ can be obtained:

$$\begin{bmatrix} \dot{r}_1 \\ \dot{r}_2 \end{bmatrix} = \begin{bmatrix} 0 & 0 \\ \dfrac{\alpha\lambda}{k_0 - \alpha} & \alpha \end{bmatrix} \begin{bmatrix} r_1 \\ r_2 \end{bmatrix} + \begin{bmatrix} -\dfrac{1}{Z_i} \\ 0 \end{bmatrix} v + \begin{bmatrix} 0 & we^{-\alpha t} \\ k_0 \left(e_0(0) - \frac{\lambda}{k_0 - \alpha} \right) e^{-(k_0 - \alpha)t} & 0 \end{bmatrix} \begin{bmatrix} r_1 \\ r_2 \end{bmatrix}. \tag{53}$$

For simplicity, (53) can be rewritten as

$$\dot{\boldsymbol{r}} = A_1 \boldsymbol{r} + Bv + A_2(t)\boldsymbol{r} \tag{54}$$

where

$$A_1 = \begin{bmatrix} 0 & 0 \\ \dfrac{\alpha\lambda}{k_0 - \alpha} & \alpha \end{bmatrix}, \quad B = \begin{bmatrix} -\dfrac{1}{Z_i} \\ 0 \end{bmatrix} \tag{55}$$

$$A_2(t) = \begin{bmatrix} 0 & we^{-\alpha t} \\ k_0 \left(e_0(0) - \dfrac{\lambda}{k_0 - \alpha} \right) e^{-(k_0 - \alpha)t} & 0 \end{bmatrix}. \tag{56}$$

For the time-varying linear system (54), we design the following state feedback controller:

$$v = \Gamma \boldsymbol{r} \tag{57}$$

where $\Gamma = [k_1, k_2] \in \mathbb{R}^{1\times 2}$ is the control gain matrix. As a consequence, the closed-loop error system is obtained as follows:

$$\dot{\boldsymbol{r}} = (A_1 + B\Gamma)\boldsymbol{r} + A_2(t)\boldsymbol{r} \tag{58}$$

where

$$A_1 + B\Gamma = \begin{bmatrix} -\dfrac{k_1}{Z_i} & -\dfrac{k_2}{Z_i} \\ \dfrac{\alpha\lambda}{k_0 - \alpha} & \alpha \end{bmatrix}. \tag{59}$$

During the visual servoing process, the height information Z_i for the selected point $\mathcal{P}_i$ is constant, and its sign can be obtained from the initial image since $Z_i = z_i X_i$ with $X_i > 0$ and z_i measurable from (5). Without loss of generality, the subsequent controller is designed with $Z_i > 0$. When $Z_i < 0$, the controller can be designed in a similar way.

Theorem 1: If the control parameters k_0 and α are chosen to satisfy

$$k_0 > \alpha > 0 \tag{60}$$

and if k_1 and k_2 are selected such that

$$\begin{cases} k_1 > 0 \\ k_2 \lambda > k_1 (k_0 - \alpha) \end{cases} \tag{61}$$

then the state of the closed-loop system (58) goes to zero with an exponential convergent rate.

Proof: Based on the the control gains condition (61), it is easy to show that $A_1 + B\Gamma$ is a Hurwitz matrix.

Besides, it follows from (56) and (60) that

$$A_2(t) \to 0 \text{ exponentially fast} \tag{62}$$

and

$$\int_0^\infty \|A_2(t)\| dt < \infty. \tag{63}$$

Therefore, using (62) and (63), we know that the origin of the second system (53) is globally exponentially stable according to the theory for time-varying linear systems with vanishing perturbation [31]. □

Based on Theorem 1, we know that

$$r_1(t), r_2(t) \longrightarrow 0 \text{ exponentially fast.} \tag{64}$$

Subsequently, from (42), (51), and (52), it is shown that

$$\rho_1(t) \to \rho_1^*, \rho_2(t) \to \rho_2^*, \theta(t) \to 0 \text{ exponentially fast.} \tag{65}$$

That is, the mobile robot is regulated to its desired pose.

Remark 2: From the proof of *Theorem 1*, it is clear that the signs of control gains k_1 and k_2 are merely related to the sign of the unknown constant Z_i. If exact knowledge of Z_i is known, the controller can be properly designed to ensure arbitrary convergence rate. Unfortunately, even through a standard adaptive controller, the parameter Z_i cannot be identified since the persistent excitation (PE) condition is not satisfied because of the simplicity of the reference signals (for example, constants for a stabilization task). Therefore, we only provide the condition for the choice of gains in (60) and (61) to ensure that the system error is convergent to zero with an exponential decaying rate, instead of constructing a further adaptive controller.

Remark 3: From the state transformation $r_2(t) = e_1(t)e^{\alpha t}$, it is shown that the measurement error of signal $e_1(t)$ is enlarged as time increases. Hence, the control performance can be possibly deteriorated when $e_1(t)$ is close to zero, since the signal-to-noise ratio is low in this case. In practical experiments, the control input is set to zero when system error is smaller than a threshold. In addition, filtering techniques for signal measurement can be further combined to suppress the noise effects.

VI. Simulation and Experimental Results

A. Simulation Results

In this section, simulation results are provided to validate the proposed approach. The landmark consists of three feature points that do

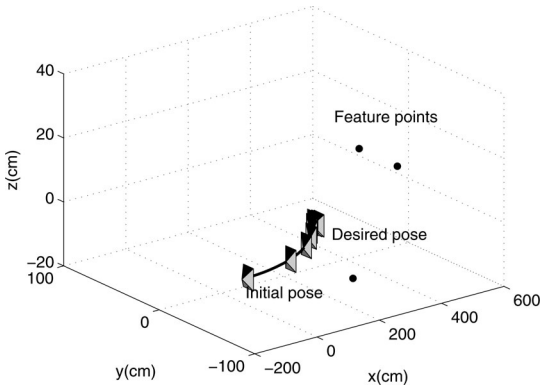

Fig. 2. Trajectory of the nonholonomic mobile robot.

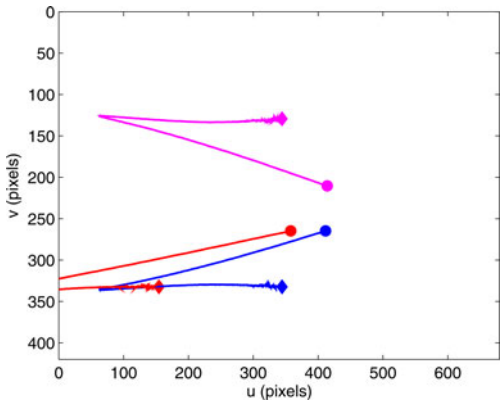

Fig. 3. Two-dimensional image trajectories of the feature points.

not lie on the same vertical plane. The initial pose of the mobile robot and the desired one are chosen as

$$x_0 = -3.8\,(\mathrm{m}), y_0 = -0.5\,(\mathrm{m}), \theta_0 = 0\,(\mathrm{deg})$$
$$x_d = 0\,(\mathrm{m}), y_d = 0\,(\mathrm{m}), \theta_d = 0\,(\mathrm{deg}). \quad (66)$$

The control gains and other parameters are chosen as follows:

$$k_0 = 0.13, k_1 = -0.0995, k_2 = -0.1050$$
$$\lambda = -0.10, \alpha = 0.07. \quad (67)$$

The camera intrinsic matrix is chosen as the parameters of a real calibrated camera. The simulated images are captured with 10 frames/s, with a resolution of 680×420 pixels. Moreover, random noise with deviation of 0.3 pixels is added into the pixel coordinates in every frame for the simulation.

Fig. 2 shows the motion trajectory of the mobile robot in 3-D scene, which is smooth in the configuration space during the visual servoing process. In Fig. 3, the corresponding 2-D image trajectory of the three feature points is illustrated, wherein the circular points denote the position of image features in the initial image, and the diamond points represent those in the desired image. It is straightforward to see that when even one of the features escapes beyond the camera FOV, the right solution can still be selected out by the use of the motion continuity, which is then utilized as feedback to drive the mobile robot to its desired pose successfully.

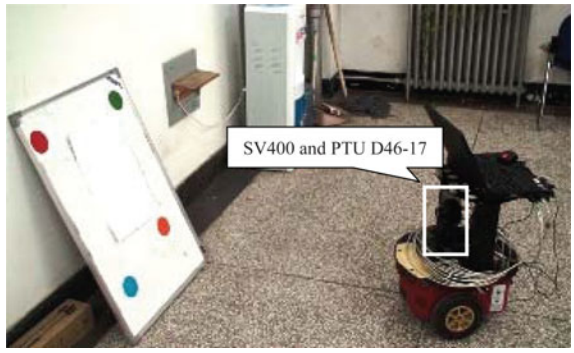

Fig. 4. Testbed.

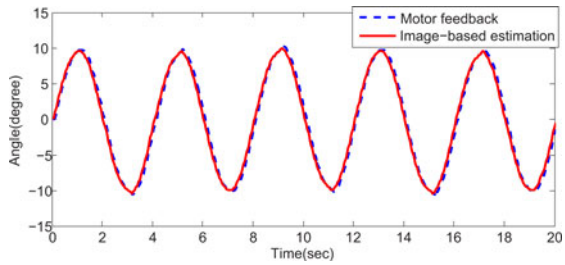

Fig. 5. Online-estimated rotational angle with amplitudes being 10°.

B. Experimental Results

In this section, two experiments are conducted to demonstrate the effectiveness of the proposed motion-estimation technique and the visual servoing strategy, respectively. As shown in Fig. 4, the vision-based robotic system is composed of a Pioneer 3-DX mobile robot that is produced by MobileRobots, Inc., and a pan-tilt unit PTU-D46-17 from Directed Perception, Inc., which is used to control the onboard digital color camera SV400 that is produced by Beijing Daheng Image Vision Company Ltd. The image sensor is a 1/2-in progressive scanning charge-coupled device with an excellent dynamic performance, which can capture 50 frames/s with a resolution of 780×582 pixels. The mobile robot, the pan-tilt unit, and the camera system are all controlled by a laptop computer through two serial ports and a firewire for communication and video transmission. Besides, the onboard camera is fixed such that the optical axis is coarsely aligned with the heading of the mobile robot when the pan-tilt unit is at its home position. To simplify the image processing step, four circular reference points with different colors are utilized as the image features that are extracted by using a thresholding algorithm. Note that we use more than three feature points to gain some robustness of the algorithm and to improve the motion-estimation results. The experiments are implemented by using OpenCV library under Visual Studio 2005.

In the first experiment, we only use the pan-tilt unit to rotate the camera along the vertical axis, while the mobile robot is kept still. The objective of this experiment is to test the accuracy of the estimated rotational angle θ by the proposed motion-estimation method, since the angle θ is directly utilized in the subsequent visual servoing strategy for feedback control. The camera is rotated along the z-axis to follow sine trajectories with different amplitudes and a fixed frequency of 0.25 Hz, and one typical experimental result is shown in Fig. 5, where the dashed lines denote the real feedback angle that has a precision of 0.05°, and the solid lines represent the computed angle by the proposed algorithm. It is shown that the performance of the motion-estimation algorithm is

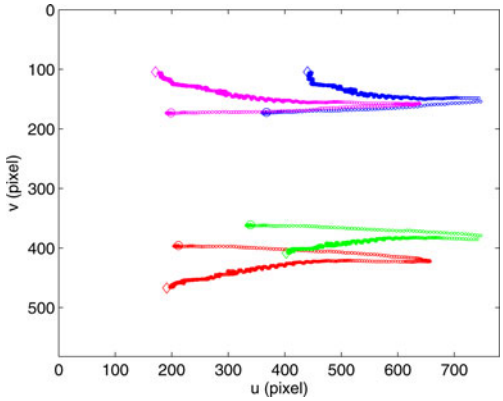

Fig. 6. Two-dimensional image trajectories of the feature points.

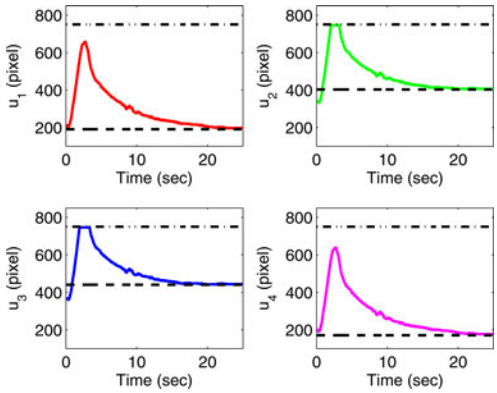

Fig. 7. Time history of pixel coordinates along the u-axis.

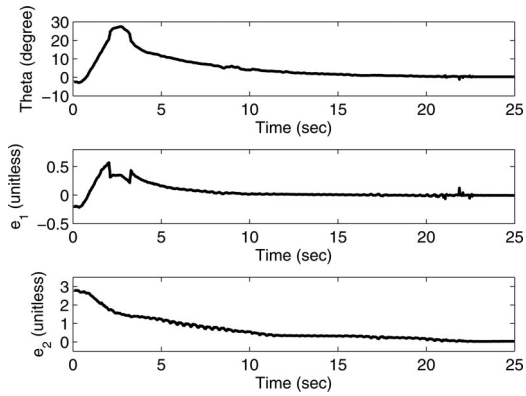

Fig. 8. System error θ, e_1, e_2.

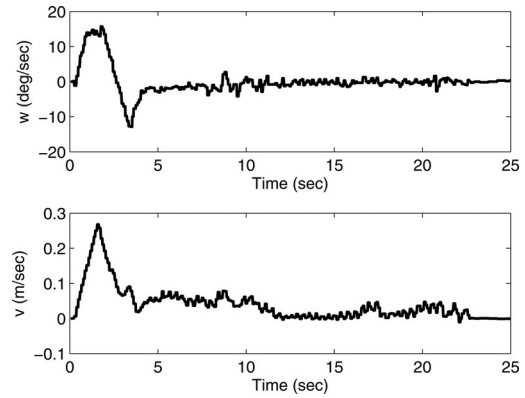

Fig. 9. Control inputs.

pretty well, and the estimation error is less than 0.3° during the motion process.

In the second experiment, we demonstrate the effectiveness of the proposed visual servoing strategy for the stabilization of a nonholonomic mobile robot, which is based on the previous verified motion-estimation technique. During this experiment, the pan-tilt unit is fixed at its home posture such that the optical axis of the camera is coarsely aligned with the heading of the mobile robot. The rough estimates of the initial and desired pose of the mobile robot with respect to the target are $(1\,\text{m}, 0\,\text{m}, 0^\circ)$ and $(2.2\,\text{m}, 0.4\,\text{m}, 3^\circ)$, and control parameters are chosen as follows:

$$k_0 = 0.13, \quad k_1 = -0.0995, \quad k_2 = -0.1050$$
$$\lambda = -0.10, \quad \alpha = 0.07. \tag{68}$$

To alleviate the effect of the time-dependent term $r_2 = e_1 e^{\alpha t}$ in the controller, the control input is set to zero when the norm of the system error $\|\boldsymbol{e}\|$ is smaller than a threshold $\epsilon = 0.01$.

The trajectory of feature points is illustrated in Fig. 6 during the visual servoing process, wherein the circular points denote the position of features in the initial image, and the diamond points represent those in the desired image. To improve the precision of the feature exaction, we assume that the feature is out of the image if $u > 750$ (pixels) or $u < 30$ (pixels) since parts of the circular areas may escape from the camera FOV in this case. Fig. 7 shows the time history of the pixel coordinates of four feature points along the u-axis, where the solid lines represent the pixel value of the image features along the u-axis in the current image, while the dashed lines denote the pixel values of the image features in the desired image and the dashed–dotted lines are referred to as the image boundary (for example, 750 pixels in this experiment). We can see that the current image gradually converges to the desired image, which implies that the robot is driven to its desired pose asymptotically. It can be seen from Fig. 7 that two features are out of the image during the servoing process; however, the relative angle can still be calculated because of the merits of the proposed motion-estimation technique. Fig. 8 shows that system error converges to zero with an exponential convergent rate. Fig. 9 shows the linear and angular velocities.

VII. Conclusion

A new 2-1/2-D visual servoing strategy for nonholonomic mobile robots is presented, which is based on a novel motion-estimation technique. The proposed approach does not require homography/fundamental matrix estimation or decomposition, and it avoids the ambiguity problem. Owing to this motion-estimation technique, the visual servoing system also gains some robustness for the FOV problem by use of the continuity property of robot movements. To incorporate the advantages of PBVS and IBVS, the system error is defined as a combination of both image signals and the rotation angle. Furthermore, a smooth time-varying pure feedback controller is designed to regulate the mobile robot to its desired pose exponentially fast, which is independent of unknown depth information. Both simulation and experimental results are provided to demonstrate the effectiveness of the proposed approach.

APPENDIX

Property 1: If two feature points $\mathcal{P}_1$ and $\mathcal{P}_2$ lie on the same perpendicular line with respect to the plane of motion, then we have $a_{12} = b_{12} = c_{12} = 0$.

Proof: For $\mathcal{P}_1$ and $\mathcal{P}_2$ on the same perpendicular line, we have

$$X_1 = X_2, \quad Y_1 = Y_2, \quad X_1^* = X_2^*, \quad Y_1^* = Y_2^*. \tag{69}$$

Hence, it is easy to know that

$$y_1 = \frac{Y_1}{X_1} = y_2, \quad y_1^* = \frac{Y_1^*}{X_1^*} = y_2^*. \tag{70}$$

Moreover, because of the planar motion of the mobile robot, the height of the features is invariant during the motion, that is

$$Z_1 = Z_1^*, \quad Z_2 = Z_2^*. \tag{71}$$

It follows from (4) and (71) that

$$\frac{z_1^*}{z_1} = \frac{X_1}{X_1^*}, \quad \frac{z_2^*}{z_2} = \frac{X_2}{X_2^*}. \tag{72}$$

According to (69), it is clear that

$$\frac{z_1^*}{z_1} = \frac{z_2^*}{z_2}. \tag{73}$$

Based on (70) and (73), it is easy to show from (22)–(24) that

$$a_{12} = 0, \quad b_{12} = 0, \quad c_{12} = 0. \tag{74}$$

The proof is completed. □

Property 2: If three feature points $\mathcal{P}_1, \mathcal{P}_2,$ and $\mathcal{P}_3$ lie in the same perpendicular plane, but any two points are not lying on the same vertical line, then the resultant constraints by any point pairs are linearly dependent.

Proof: Without loss of generality, we only prove that the constraint by $(\mathcal{P}_1, \mathcal{P}_3)$ and the constraint by $(\mathcal{P}_2, \mathcal{P}_3)$, are linearly dependent. In other words, vectors $(a_{12}, b_{12}, c_{12})^{\mathrm{T}}$ and $(a_{13}, b_{13}, c_{13})^{\mathrm{T}}$ are linearly dependent.

Since the three points lie in a same perpendicular plane with respect to the xy plane, but any two points do not lie on a same vertical line, we can obtain three different points on the intersection line of the perpendicular plane and xy plane through orthogonal projection. Thus, there exists a constant $\delta \in \mathbb{R}$ and $\delta \neq 0$ such that the following relationships hold:

$$\begin{bmatrix} X_3^* \\ Y_3^* \end{bmatrix} = (1-\delta) \begin{bmatrix} X_1^* \\ Y_1^* \end{bmatrix} + \delta \begin{bmatrix} X_2^* \\ Y_2^* \end{bmatrix}. \tag{75}$$

Substituting (4) into (22), we know that

$$a_{13} = \frac{Y_1 Y_3}{X_1^* X_3^*} + \frac{X_1}{X_1^*} - \frac{Y_1^* Y_3}{X_3^* X_1^*} - \frac{X_3}{X_3^*}. \tag{76}$$

To express X_1, Y_1, X_3, Y_3 by the desired coordinates $X_1^*, Y_1^*, X_3^*, Y_3^*$, (8) can be utilized to obtain

$$a_{13} = 2\left(\frac{Y_3^*}{X_3^*} - \frac{Y_1^*}{X_1^*}\right)\sin(\theta) + t_x\left(\frac{1}{X_1^*} - \frac{1}{X_3^*}\right) + \frac{t_y}{X_1^* X_3^*}\left(Y_3^* - Y_1^*\right). \tag{77}$$

In a similar way, we can show that

$$a_{12} = 2\left(\frac{Y_2^*}{X_2^*} - \frac{Y_1^*}{X_1^*}\right)\sin(\theta) + t_x\left(\frac{1}{X_1^*} - \frac{1}{X_2^*}\right) + \frac{t_y}{X_1^* X_2^*}\left(Y_2^* - Y_1^*\right). \tag{78}$$

It follows from (75) that

$$\begin{aligned} \frac{Y_3^*}{X_3^*} - \frac{Y_1^*}{X_1^*} &= \left(\frac{Y_3^*}{X_3^*} - \frac{Y_1^*}{X_3^*}\right) + \left(\frac{Y_1^*}{X_3^*} - \frac{Y_1^*}{X_1^*}\right) \\ &= \frac{\delta(Y_2^* - Y_1^*)}{X_3^*} + Y_1^* \frac{\delta(X_1^* - X_2^*)}{X_1^* X_3^*} \\ &= \delta \frac{X_2^*}{X_3^*}\left(\frac{Y_2^*}{X_2^*} - \frac{Y_1^*}{X_1^*}\right). \end{aligned} \tag{79}$$

Similarly, we have

$$\frac{1}{X_1^*} - \frac{1}{X_3^*} = \delta \frac{X_2^*}{X_3^*}\left(\frac{1}{X_1^*} - \frac{1}{X_2^*}\right) \tag{80}$$

$$\frac{1}{X_1^* X_3^*}\left(Y_3^* - Y_1^*\right) = \delta \frac{X_2^*}{X_3^*} \cdot \frac{1}{X_1^* X_2^*}\left(Y_2^* - Y_1^*\right). \tag{81}$$

From (77), (78), (79), (80), and (81), it is easy to show that

$$a_{13} = \delta \frac{X_2^*}{X_3^*} a_{12}. \tag{82}$$

After some mathematical manipulation, we can also show that

$$b_{13} = \delta \frac{X_2^*}{X_3^*} b_{12}, \quad c_{13} = \delta \frac{X_2^*}{X_3^*} c_{12}. \tag{83}$$

Therefore, vectors $(a_{12}, b_{12}, c_{12})^{\mathrm{T}}$ and $(a_{13}, b_{13}, c_{13})^{\mathrm{T}}$ are linearly dependent. □

REFERENCES

[1] S. Hutchinson, G. Hager, and P. I. Corke, "A tutorial on visual servo control," *IEEE Trans. Robot. Autom.*, vol. 12, no. 5, pp. 651–670, Oct. 1996.

[2] F. Chaumette and S. Hutchinson, "Visual servo control—Part I: Basic approaches," *IEEE Robot. Autom. Mag.*, vol. 13, no. 4, pp. 82–90, Dec. 2006.

[3] F. Chaumette and S. Hutchinson, "Visual servo control—Part II: Advanced approaches," *IEEE Robot. Autom. Mag.*, vol. 14, no. 1, pp. 109–118, Mar. 2007.

[4] R. W. Brockett, "Asymptotic stability and feedback stabilization," in *Differential Geometric Control Theory*, R. W. Brockett, R. S. Millman, and H. J. Sussmann, Eds. Boston, MA: Birkhäuser, 1983, pp. 181–191.

[5] A. Astolfi, "Discontinuous control of nonholonomic systems," *Syst. Control Lett.*, vol. 27, no. 1, pp. 37–45, 1996.

[6] N. Marchand and M. Alamir, "Discontinuous exponential stabilization of chained form systems," *Automatica*, vol. 39, pp. 343–348, 2003.

[7] A. M. Bloch, M. Reyhanoglu, and N. H. McClamroch, "Control and stabilization of nonholonomic dynamic systems," *IEEE Trans. Automat. Contr.*, vol. 37, no. 11, pp. 1746–1757, Nov. 1992.

[8] J. M. Coron, "Global asymptotic stabilization for controllable systems without drift," *Math. Control, Signals Syst.*, vol. 5, pp. 295–312, 1991.

[9] Y. P. Tian and S. Li, "Exponential stabilization of nonholonomic dynamic systems by smooth time-varying control," *Automatica*, vol. 38, pp. 1139–1146, 2002.

[10] H. Yuan and Z. Qu, "Continuous time-varying pure feedback control for chained nonholonomic systems with exponential convergent rate," in *Proc. 17th Int. Federation Atomic Control World Congr.*, Seoul, Korea, 2008, pp. 15203–15208.

[11] Y. Hu, S. S. Ge, and C. Su, "Stabilization of uncertain nonholonomic systems via time-varying sliding mode control," *IEEE Trans. Autom. Control*, vol. 49, no. 5, pp. 757–763, May 2004.

[12] O. J. Sørdalen and O. Egeland, "Exponential stabilization of nonholonomic chained systems," *IEEE Trans. Autom. Control*, vol. 40, no. 1, pp. 35–49, Jan. 1995.
[13] Y. Masutani, M. Mikawa, N. Maru, and F. Miyazaki, "Visual servoing for non-holonomic mobile robots," in *Proc. IEEE/RSJ Int. Conf. Intell. Robots Syst*., 1994, vol. 2, pp. 1133–1140.
[14] K. Hashimoto and T. Noritsugu, "Visual servoing of nonholonomic cart," in *Proc. IEEE Int. Conf. Robot. Autom*., 1997, pp. 1719–1724.
[15] N. Gans and S. Hutchinson, "A stable vision-based control scheme for nonholonomic vehicles to keep a landmark in the field of view," in *Proc. IEEE Int. Conf. Robot. Autom*., 2007, pp. 2196–2201.
[16] P. Murrieri, D. Fontanelli, and A. Bicchi, "A hybrid-control approach to the parking problem of a wheeled vehicle using limited view-angle visual feedback," *Int. J. Robot. Res*., vol. 23, no. 4–5, pp. 437–448, 2004.
[17] M. Aicardi, G. Casalino, A. Bicchi, and A. Balestrino, "Closed loop steering of unicycle-like vehicles via Lyapunov techniques," *IEEE Robot. Autom. Mag*., vol. 2, no. 1, pp. 27–35, Mar. 1995.
[18] G. L. Mariottini, G. Oriolo, and D. Prattichizzo, "Image-based visual servoing for nonholonomic mobile robots using epipolar geometry," *IEEE Trans. Robot*., vol. 23, no. 1, pp. 87–100, Feb. 2007.
[19] G. López-Nicolás, C. Sagüés, J. J. Guerrero, D. Kragic, and P. Jensfelt, "Switching visual control based on epipoles for mobile robots," *Robot. Autonom. Syst*., vol. 56, no. 7, pp. 592–603, 2008.
[20] G. López-Nicolás, C. Sagüés, and J. J. Guerrero, "Parking with the essential matrix without short baseline degeneracies," in *Proc. IEEE Int. Conf. Robot. Autom*., Kobe, Japan, May 12–17, 2009, pp. 1098–1103.
[21] R. I. Hartley and A. Zisserman, *Multiple View Geometry in Computer Vision*. New York: Cambridge Univ. Press, 2000.
[22] Y. Fang, W. E. Dixon, D. M. Dawson, and P. Chawda, "Homography-based visual servo regulation of mobile robots," *IEEE Trans. Syst. Man Cybern.—Part B: Cybern*., vol. 35, no. 5, pp. 1041–1050, Oct. 2005.
[23] J. Chen, W. E. Dixon, D. M. Dawson, and M. McIntyre, "Homography-based visual servo tracking control of a wheeled mobile robot," *IEEE Trans. Robot*., vol. 22, no. 2, pp. 406–415, Apr. 2006.
[24] O. Faugeras and F. Lustman, "Motion and structure from motion in a piecewise planar environment," *Int. J. Pattern Recognit. Artif. Intell*., vol. 2, no. 3, pp. 485–508, 1988.
[25] X. Zhang, Y. Fang, B. Ma, and X. Liu, "A fast homography decomposition technique for visual servo of mobile robots," in *Proc. Chinese Control Conf*., vol. 5, Kunming, China, 2008, pp. 404–409.
[26] G. López-Nicolás, S. Bhattacharya, J. J. Guerrero, C. Sagüés, and S. Hutchinson, "Switched homography-based visual control of differential drive vehicles with field-of-view constraints," in *Proc. IEEE Int. Conf. Robot. Autom*., 2007, pp. 4238–4244.
[27] X. Zhang, Y. Fang, and X. Liu, "Visual servoing of nonholonomic mobile robots based on a new motion estimation technique," in *Proc. IEEE Conf. Decis. Control*, Shanghai, China, Dec. 2009, pp. 8428–8433.
[28] Z. Zhang, "A flexible new technique for camera calibration," *IEEE Trans. Pattern Anal. Mach. Intell*., vol. 22, no. 11, pp. 1330–1334, Nov. 2000.
[29] J. Oliensis, "Exact two-image structure from motion," *IEEE Trans. Pattern Anal. Mach. Intell*., vol. 24, no. 12, pp. 1618–1633, Dec. 2002.
[30] G. Chesi and K. Hashimoto, "A simple technique for improving camera displacement estimation in eye-in-hand visual servoing," *IEEE Trans. Pattern Anal. Mach. Intell*., vol. 26, no. 9, pp. 1239–1242, Sep. 2004.
[31] H. K. Khalil, *Nonlinear Systems*, 3rd ed. Englewood Cliffs, NJ: Prentice-Hall, 2002.